Directional response of several geometries for reactor-neutrino detectors

Mark J. Duvall,* Brian C. Crow, Max A.A. Dornfest, and John G. Learned
Department of Physics and Astronomy, University of Hawai'i at Mānoa

Marc F. Bergevin, Steven A. Dazeley, and Viacheslav A. Li
Lawrence Livermore National Laboratory

(Received 13 February 2024; revised 1 August 2024; accepted 20 September 2024; published 12 November 2024)

We have modeled six abstracted detector designs, with the goal of determining their ability to resolve the direction to an antineutrino source, including two for which we have operational data for validating our computer modeling and analytical processes. We have found that the most promising options, regardless of scale and range, have angular resolutions on the order of a few degrees, which is better than any yet achieved in practice by a factor of at least two. We examine and compare several approaches to detector geometry for their ability not only to detect the inverse beta decay (IBD) reaction, but also to determine the source direction of incident antineutrinos. The information from these detectors provides insight into reactor power and burning profile, which is especially useful in constraining the clandestine production of weapons material. In a live deployment, a nonproliferation detector must be able to isolate the subject reactor, possibly from a field of much-larger power reactors; directional sensitivity can help greatly with this task. We also discuss implications for using such detectors in longer-distance observation of reactors, from a few kilometers to hundreds of kilometers.

DOI: 10.1103/PhysRevApplied.22.054030

I. INTRODUCTION

The first detection of neutrinos (specifically, in the form of electron-antineutrinos) was accomplished by Cowan *et al.* in the mid 1950s [1]. Rapidly thereafter, neutrinos were observed from cosmic rays (South Africa [2] and Kolar gold mines [3]); they were also observed at accelerators (Brookhaven [4]). Many observations were performed successfully in the proximity of reactors around the world. In parallel, solar neutrinos were observed in the Homestake mine [5]. Through these experiments and others, weak-interaction theory was validated. Limits were set on neutrino mass, neutrino stability, and the number of neutrino types.

Soon thereafter, in the 1960s and the 1970s, commercial power reactors began producing power in quantities enough to start considering reactor neutrinos specifically [6] as a neutrino-oscillation study tool. In the 1980s and early 1990s, there were a number of experiments at reactors carried out at multiple baselines to look for neutrino-oscillation effects (Rovno [7], Gösgen [8], Bugey [9], Krasnoyarsk [10], and Savannah River [11]). In 1998, SuperKamiokande detected the first clear example of neutrino oscillations via the disappearance of cosmic-ray muon neutrinos traversing the Earth [12], setting off the modern avalanche of neutrino studies. Next, the SNO experiment found evidence of both solar electron-neutrino disappearance and total solar-neutrino conservation via observation of the unsuppressed neutral-current solar-neutrino interactions [13,14]. In 2003, the KamLAND experiment detected the disappearance of neutrinos from the ensemble of reactors around Japan, producing the first unequivocal evidence that electron-neutrinos oscillate [15]. This cemented the case for oscillatory neutrino flavor changing, explaining the decades-long solar-neutrino quandary.

The subject of using antineutrinos in the nonproliferation context has seen a renaissance in the recent years [16,17]. In the near-field and mid-field, the community has entered a precision era, as seen with PROSPECT [18] and DayaBay [19,20]. Long-range detection is becoming possible; with the undoped liquid scintillator KamLAND [15] and water SNO+ detector [21], as well as the JUNO and the gadolinium-doped SuperKamiokande detectors, all coming online.

In the early 2010s, an interest in studies on short-baseline neutrinos was rejuvenated with a series of papers describing a few-percent deficit observed by previous experiments due to reevaluated antineutrino flux. This so-called reactor-antineutrino anomaly [22] led scientists to propose some new detectors such as PROSPECT [23], SOLID [24], miniChandler [25], and NuLat [26]. Other

*Contact author: mjduvall@hawaii.edu

segmented detectors that have been in operation since around that time include DANSS [27] and PANDA [28]. Although the anomaly has since been resolved through improved measurements of the beta spectra [29], this plethora of experiments as a result of the hunt for solving the anomaly put us in an era of experiments that can measure antineutrino spectrum with high precision and could be operated above-ground with not much overburden. Currently, in the mid 2020s, this era continues with scientists looking for ways to use these new tools for safeguarding nuclear reactors [30,31].

For large detectors in the nonproliferation context, directionality, or the ability to reconstruct the direction of the antineutrino source, has been proposed as a useful capability to determine the source of a clandestine reactor [32]. The concept was first presented by the Double Chooz experiment in 2007. Using a sample of 2500 events they report an angular resolution corresponding to resolving a neutrino source to within a 1σ half-cone aperture of 2.3° [33]. Expected utility is in small modular reactors where the detector could, in principle, distinguish neutrinos coming from multiple cores [34]. While we look forward to publishing results with background environments in the future, it remains critical to note that this current work does not include backgrounds. Quantification of detector geometry to signal generation is the hallmark of this study.

II. DIRECTIONALITY FROM INVERSE BETA DECAY

We start by defining the coordinate system used herein. Under the assumption that the reactors in question are located in the same horizontal plane as the detector (neither in the sky nor deep underground relative to the observation point), we focus on determination of the azimuthal direction:

$$\varphi_\nu = \arctan\left(\frac{p_{\nu\perp}}{p_{\nu\parallel}}\right) = \arctan\left(\frac{\Delta y}{\Delta x}\right), \tag{1}$$

$$\varphi \equiv 180^\circ - \varphi_\nu. \tag{2}$$

In detector physics, *directionality* refers to the ability of a detector to determine the incident direction of an incoming particle, and by extension to infer the direction pointing from the detector to the particle's source. Figure 1 illustrates this concept as applied to a detector attempting to reconstruct the direction $\hat{S}_T$ to the source of the incoming antineutrinos. The source is assumed to be located on the horizon relative to the detector (i.e., $z_{\text{Detector}} = z_{\text{Source}}$), so this problem reduces to reconstructing the azimuthal angle φ, which can be found as given in Eqs. (1) and (2). Note that some of the background from distant reactors will be substantially out-of-plane, so we get some small relief from backgrounds which are due to reactors located well

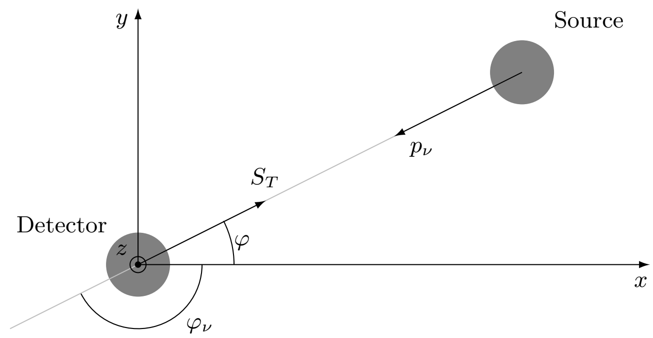

FIG. 1. Key directional quantities (xy projection). The vector S_T is a vector indicating the true direction toward the source. In this study, all antineutrinos are assumed to have the same direction in their momentum p_ν.

below the horizon. This effect is mostly relevant for large, long-baseline detectors [35].

These can be seen in Sec. IV (Fig. 3).

A. Acquisition

The key task for inverse beta decay (IBD) directionality is therefore to find the direction of the neutron's momentum as it exits the IBD vertex. In practice, this is achieved by finding the average direction of neutron displacement from production to capture over a set of events.

The displacement of the e^+ from its production (which is at the IBD vertex) to its annihilation is typically much shorter than the capture displacement of the n, so we can reliably use a point along the e^+ track to approximate the location of the IBD vertex. In other words, the short distance between the IBD vertex and the end of the e^+ track is negligible compared with the neutron-capture distance. (In fact, it is so short that it has generally been irresolvable in practice.) The method for extracting directional information from an IBD detector is then to draw a vector from the location of neutron capture to the location of the positron event. This vector, which we denote as $\vec{S}_R$, represents the reconstructed direction to the antineutrino source. The true direction from the detector back to the antineutrino source will be indicated by the unit vector $\hat{S}_T$. In a directionally sensitive detector, the average of $\hat{S}_R$ over a large number of events will increasingly tend toward $\hat{S}_T$.

The magnitude $\|\vec{S}_R\|$ gives us the approximate capture distance of the neutron, which we will hereafter denote as d_n (i.e., $d_n \equiv \|\vec{S}_R\|$). We are sometimes interested in this, but for directional purposes it is often convenient to simply use the corresponding unit vector, $\hat{S}_R$. We can also define the quantity ψ as the angle between $\hat{S}_R$ and $\hat{S}_T$, as shown in Fig. 2 and according to the following: $\cos\psi = \hat{S}_R \cdot \hat{S}_T$. Our work verified the expected theoretical curve, via simulation, as shown in Fig. 3.

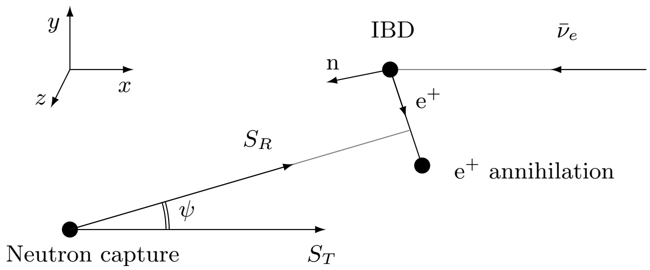

FIG. 2. How the angle ψ between reconstructed S_R and true S_T source direction is defined. The vector S_R points from the reconstructed vertex of the neutron capture toward the reconstructed vertex where positron deposited its energy before annihilating. The megaelectronvolt-scale positron travels a few millimeters before being annihilated with an electron. The kiloelectronvolt-scale neutron loses its energy in the detector medium before being captured; the separation between IBD vertex and the capture location could be made large if there is no medium in between, as in some of the detector designs considered in this study. The antineutrino source was positioned along the x-axis: angle $\psi = 0$ would indicate a perfect reconstruction of direction.

B. Statistics

The determination of the direction of the incoming antineutrino is an inherently stochastic process. This is because of the scattering undergone by the neutron during its moderation/thermalization phase. This scattering is a *nearly* isotropic random walk after the first scatter, with only a slight bias in the forward direction of antineutrino travel. The capture displacement of the neutron (and consequently $\hat{S}_R$) for any particular event will then be in a nearly random direction, and it is therefore only the average of $\hat{S}_R$ over a substantial number of events that will reliably point in a direction near $\hat{S}_T$ and give a meaningful result for the direction to the antineutrino source. This is true even for cases in which the n-scattering region can be separated from the e^+-track region, as discussed in detail in Sec. III B. The results in [36] also indicate that, on average, the e^+ will have a slight bias to leave the IBD interaction heading in the backward direction relative to the incoming $\overline{\nu_e}$.

C. Neutron-capture agent

The dopant isotope determines the interevent time and both the energy and degree of localization for the delayed event, along with a host of other design considerations. Common dopant isotopes include ^{6}Li, ^{10}B, and ^{155}Gd/^{157}Gd, all three of which are used in this study. Neutron captures on ^{1}H are also common, simply because frequently used target materials such as water and organic molecules contain hydrogen. The natural isotopic abundances and capture reactions are included in the simulations [37–40]. In the simulation, we keep the by-weight

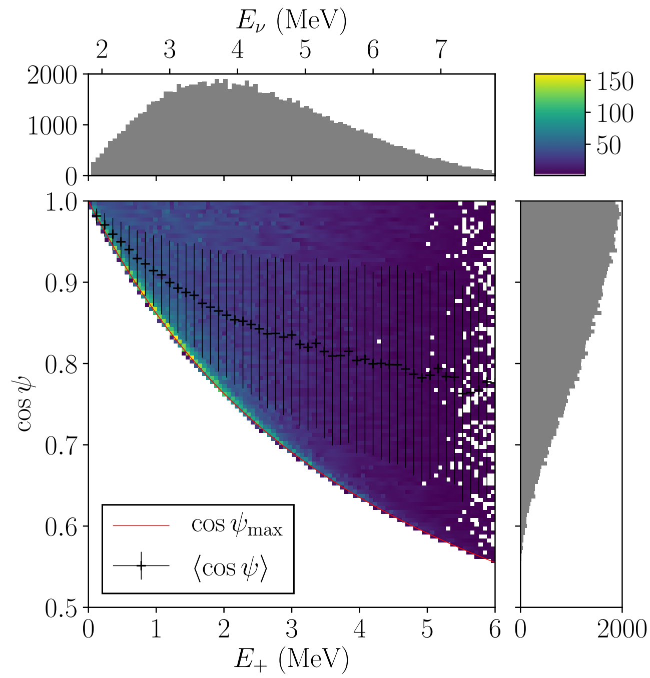

FIG. 3. Distribution of positron kinetic energy E_+ and cosine of neutron scattering angle ψ relative to the incoming antineutrino, based on simulating 100 000 IBD positron-neutron pairs. The binning in both axes, cos ψ and positron energy E_+, is 100; the projections are shown in gray in the inset 1D histograms. The mean values and standard deviations, along with the analytical calculation for the maximum angle, are also displayed. It is worth noting that the 2D distribution has a sharp peak when the angle approaches the maximum allowed angle (shown as a red curve), resulting in the shift of the mean value toward that curve. Simulated via RAT-PAC.

doping levels as follows: 0.1% for Gd-doped detectors; 1.5% for ^{6}Li; and 5% for ^{10}B.

D. Relation to other designs

The forward/backward asymmetry in IBD neutrons was first discovered by Gabrielle Zacek by analyzing data from the Gösgen experiment [41]. The effect was also observed by Palo Verde [42] and Bugey 3. The first experiment to successfully demonstrate directional detection of electron antineutrinos via IBD was the Chooz experiment, which used approximately 2700 IBD events to “[locate] an antineutrino source to within a cone of half-aperture ≈22° at the 68% C.L.” (confidence level) [43]. The Double Chooz (DC) experiment then improved on this result, acquiring ∼8200 IBD events and reducing the cone to half-aperture ≈6° [44,45].

1. Concurrent and future

Other collaborations working along these lines include the PROSPECT [18] and Daya Bay experiments; both have published their final measurements last year [19,20].

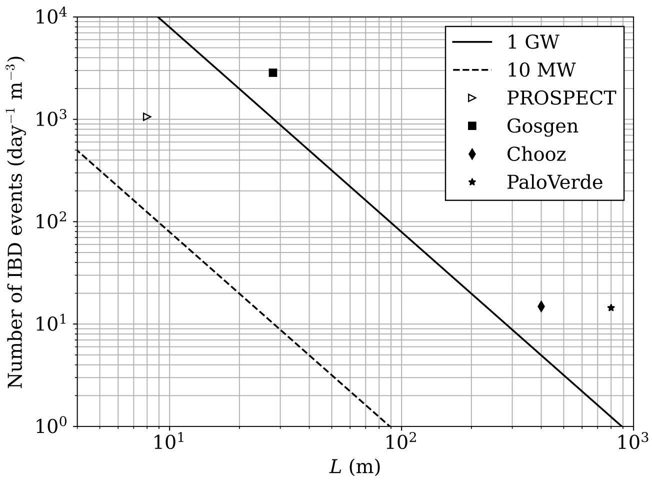

FIG. 4. Number of IBD interactions per day per cubic meter of detector volume, using a detector medium with 5×10^{22} cm^{-3} number density for hydrogen. Various power and research reactors cited previously are featured as test points. Note that upward on the plot is equivalent to increasing reactor power.

The RENO [46] (Korea), Double Chooz [47] (France), and Borexino [48] experiments have also concluded. KamLAND and SuperKamiokande are operating, but neither has the resolution to resolve IBD directions. The JUNO project in China is under construction and hopefully will soon operate. Due to the small ($\approx 5 \times 10^{-43}$ cm^2) cross section for IBD, large detector volumes are needed to get sufficient numbers of events for directional reconstruction with good statistics, as shown in Fig. 4.

III. METHODOLOGY

A. Simulated detectors

1. Monolithic

Because of the success of Double Chooz as mentioned previously, we have chosen it as a basis for comparison in this study. In Chooz and Double Chooz, as well as other major antineutrino experiments such as RENO [46] and Daya Bay [49], all of the target material is arranged in a single, central volume. We will hereafter refer to this basic design as the *monolithic* type. This volume is usually a simple geometric shape such as a sphere, cube, or cylinder. Choosing such highly symmetric configurations simplifies reconstruction of the interaction locations.

In a monolithic detector such as Double Chooz, the prompt and delayed events take place in a single, continuous volume which is large compared with the distance traveled by the neutron. The positions of the positron and neutron events are then reconstructed using the relative time and/or charge registered by photomultiplier tubes (PMTs) which are spread over the surface of the volume. The version of this geometry that we implemented is a right cylinder tank 10 m in diameter and 10 m in height; note that it is considerably larger than the tanks used in the actual Double Chooz experiment.

2. Segmented 3D: NuLat

A key limitation of the monolithic approach is that its spatial resolution is typically larger than the neutron displacement needed to infer the source direction. This means that the most immediate factor limiting the directional capability of a monolithic detector is its spatial resolution. The basic concept behind the *segmented* approach is to improve the spatial resolution by dividing the target volume into a lattice of cells which are each smaller than the desired distance measurement.

For our example segmented design, we chose the Neutrino Lattice (NuLat) detector [26], in which the target volume is a cube subdivided into cubical cells. Interaction positions can then be determined to a resolution corresponding to the size of the cells. The trick then lies in identifying which cell is active at a particular time. NuLat accomplishes this by employing total internal reflection (TIR) to create what is known as a Raghavan Optical Lattice (ROL). The TIR is made possible by a 1-mm air gap between scintillator segments. Light is channeled along each of the three principal axes from the originating cell to the outer faces, which would be instrumented with PMTs. Combining the information from each face reveals the $\{x, y, z\}$ of the originating cell.

Directional information from IBD interactions comes from events in which the prompt and delayed events occur in different cells; $\vec{S}_R$ is then simply a vector from the center of the first cell to the center of the second. This also indicates that the cell dimensions should be comparable to the typical neutron travel distance (d_n) in the target material. For this study, the cells were 5-cm cubes, comparable to the few-centimeter capture distances typical of our chosen materials. The simplest configuration, $3 \times 3 \times 3$, gives one central cell with a neighbor in every direction; this is the configuration used in our Monte Carlo (MC) simulations and is shown in Fig. 5. The NuLat demonstrator [50] that was built was $5 \times 5 \times 5$, and the actual NuLat is planned for $15 \times 15 \times 15$ [26].

3. Segmented 2D: SANDD

Another recent segmented detector design is Segmented Anti-Neutrino Directional Detector (SANDD), a small (6.4-liter) array of ^{6}Li-doped plastic scintillators with pulse-shape discrimination (PSD) capability [51]. (PSD makes it possible to distinguish certain particle types based on the shape of their scintillation pulses.) A prototype was designed and built for exploring near-field reactor monitoring, including sensitivity to IBD antineutrino direction. The core concept is an 8×8 bundle of square scintillating rods (5.4 mm $\times$ 5.4 mm $\times$ 40.64 cm) to detect both the initial interaction and the neutron capture. This

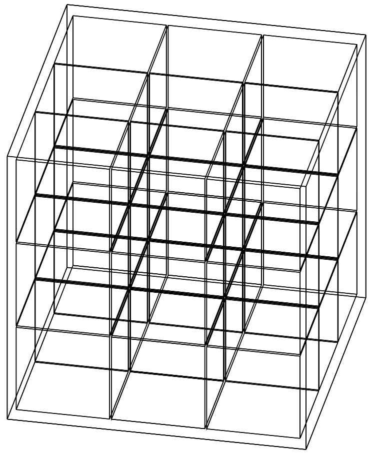

FIG. 5. Simulated NuLat 3^3 geometry: a $3 \times 3 \times 3$ array of ^{6}Li-doped scintillator cubes. The cubes have a 5-cm side length and are separated by a 1-mm air gap. For this arrangement, the IBD interaction vertices (and, therefore, the prompt events) are restricted to the central cube only; but the delayed events can occur in any of the 27 cubes.

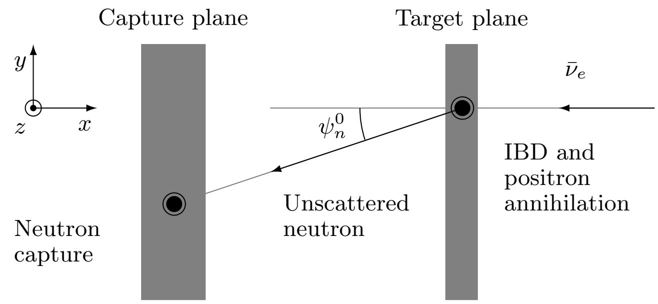

FIG. 6. Design concept of a target-capture-plane detector based on the SANTA. In this study, the antineutrino direction was perpendicular to the detector planes. Only one capture plane was implemented (unlike the original design with the second capture plane). Angle ψ_n^0 is the angle between the direction of capture-IBD cells and the x-axis. In the separation detector, like SANTA, the mean values for angles ψ_n^0 and φ are the same.

inner core of rods (hereafter referred to as the SANDD central module, or "SANDD-CM") is designed to be surrounded by a single layer of square 2.54-cm scintillating bar segments and an additional layer of scintillating slabs (2.54 cm $\times$ 5.08 cm). The configuration is quite similar to the Double Scatter Neutrino Camera built and tested at UH, as part of the program to study a Single Volume Scatter Camera for neutron direction determination, hosted by Livermore/SANDIA [52]. We estimated that this prototype would have needed enlarging to ton-scale fiducial volume to have enough sensitivity for useful observations near a reactor, but it did show promising performance in lab tests. The NuLat and SANDD prototypes have demonstrated the viability of utilizing an array of scintillating parallelpipeds for IBD detection, but they have also highlighted the problem of requiring many detector and electronics channels ($\sim 10^4$ or more) when scaling up to the required fiducial volumes for reactor studies, even from a distance of a few meters.

B. Resolving the neutron-scattering problem

A fundamental challenge for any IBD detector is that neutron scattering quickly degrades directionality. IBD neutrons do not have a uniform initial direction (even if the incident antineutrinos do), so they were not well-suited to illustrate the directionality effect at the IBD energies. At this point, the neutron-scattering process becomes the dominating factor limiting improvements in the angular resolution of the detector. We ran a set of neutron-only simulations specifically to illustrate this process; those results are discussed in Sec. IV (see, in particular, Fig. 8).

The loss of directional information due to neutron scattering is an inherent limitation in bulk-volume detectors, whether they are monolithic like Double Chooz or subdivided like NuLat. One proposed solution to this problem is the Segmented AntiNeutrino Tomography Apparatus (SANTA) [53], which allows the neutron to travel much further in its original direction before its first scatter. This requires the neutron to leave the target material almost immediately after it is produced, then travel some relatively long distance, then enter a second volume of target material and capture there. As shown in Fig. 6, SANTA proposes to achieve this by arranging the scintillator materials into two separate layers: a very thin "target" layer for the prompt event and neutron production, and a thicker "capture" layer for neutron thermalization and capture. In order to encourage the neutron to capture in the correct layer, the target layer would not be doped with any neutron-capture agents, and the capture layer would be doped rather heavily: for example, polyvinyl toluene (PVT) at 5 wt % natural boron in the original proposal.

The dramatic benefit of this approach is that neutron scattering has only a minimal effect on the reconstructed source direction. This can be seen in Fig. 6. In most IBD detectors, the neutron-capture region surrounds the IBD vertex, and the randomness of the neutron's scattering almost completely determines the angle φ. SANTA sidesteps this problem by moving the scattering downstream, so that n captures anywhere within the scattering region will point approximately along the true source direction. We refer to this target-segment $\rightarrow$ flight $\rightarrow$ capture-segment arrangement as a *separation* detector.

It is worth noting that the neutron is not guaranteed to capture in the capture layer, even with heavy doping. A neutron may, for example, bounce off of the capture layer and eventually capture back in the target layer, possibly reflecting off of nearby walls or shielding in the process.

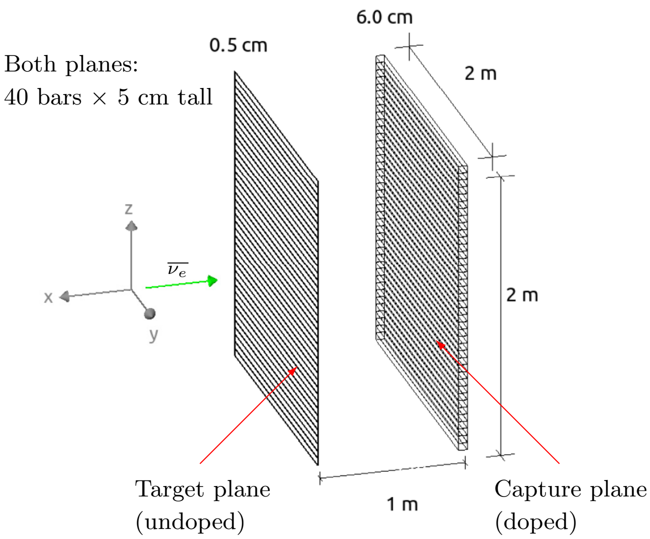

FIG. 7. Simulated SANTA Geometry: the "target" plane composed of 40 bars of undoped scintillator 2 m × 0.05 m × 0.005 m; the "capture" plane composed of 40 scintillator bars doped with natural boron, 2 m × 0.05 m × 0.06 m. The separation between the two planes is 1 m, resulting in a "packing factor" of about 0.46% (the ratio of the target volume to the total volume of the detector).

(Such captures typically occur on an ^{1}H in the plastic.) These relatively rare events could still be used to measure the total antineutrino rate but would generally be cut from the directional analysis.

The implementation of SANTA used in this MC study was based on a possible realization proposed in [53]. It contains a 0.5-cm-thick undoped target layer separated by 1 m from a 6-cm-thick capture layer doped at 5 wt% natural boron, as shown in Fig. 7. Both layers are composed of PVT plastic scintillator and are 2 m × 2 m. The original proposal included an additional layer, upstream of the target layer, for catching positrons that escape the target layer. We elected to forego this feature, both to keep the configuration minimal and because the energy deposition from positron tracks in the target layer was sufficient for our purposes. No explicit mechanism was proposed by [53] for measuring the locations of the interactions in the scintillator. At University of Hawai'i (UH), we took this concept and considered how it might be realized in an actual detector. To this end, we subdivided each plane into a set of 40 horizontal scintillator bars, each 50 mm tall and separated by 1 mm from the next bar. We inserted a 0.5-mm strip of black acrylic for optical separation between each bar. In a real detector, a 5-cm PMT or silicon photomultiplier (SiPM) would then be placed at either end of each bar, for a total of 160 light sensors. For a typical prompt or delayed event, a strong signal will be produced in exactly one bar. The event's position can then be extracted as follows. The vertical component (z) is taken to be the value of z at the center of the bar. The axial component (x) is taken to be the value of x at the center of the plane (so, in our implementation, $x = \mp 50$ cm for the target/capture plane). The transverse component (y) is determined by comparing light output at either end of the bar. If fast-timing measurements are available, the transverse determination could be enhanced by comparing photon arrival times at either end of the bar.

Finally, SANTA is unique among the designs studied here in that it does not have a full field of view (FOV); that is, it is sensitive only to antineutrinos coming generally from its "forward" direction ($+x$ in Figs. 6–8. This does bias the results: SANTA will always report a source direction within its FOV. We have run preliminary simulations using off-axis neutron beams; the results suggest that, after accounting for a systematic skew toward the center, SANTA can reliably identify off-axis sources within its FOV. More specifically, SANTA's FOV is approximately a cone (3D) or arc (2D) of half-angle 45°. This is ~15% of 4π sr in three dimensions and exactly 25% of 2π rad in two dimensions. Whether this limited FOV is a drawback or a benefit depends on the objective of a given deployment. For example, it is clearly detrimental if attempting to locate an unknown reactor with an arbitrary position; but it can suppress noise from irrelevant directions if attempting detailed measurements near a known reactor.

C. Hybrid

1. Motivation

Our collaboration felt that the SANTA approach featured an ingenious insight on solving the aforementioned neutron-scattering problem; however, we also anticipated some major practical limitations with the design as laid out in the original paper. Our two biggest concerns were that, relative to the more traditional designs:

(1) the much-larger surface-area-to-volume ratio would expose the detector to severe levels of backgrounds, especially in our targeted near-surface deployment scenario;

(2) the much-smaller target-volume-to-footprint ratio would severely restrict the achievable target mass in a real deployment environment.

It is worth noting that the SANTA design does inherently compensate somewhat for both of these effects, in that it requires many fewer events to achieve a given angular resolution. However, our simulations indicated that this compensation alone would likely be insufficient to make the original design practically viable.

We therefore set out to devise a class of detector designs that would strike a balance between the directional performance of SANTA and the larger target mass and stronger resilience against backgrounds of the more-traditional detectors. In this work, we refer to such detector

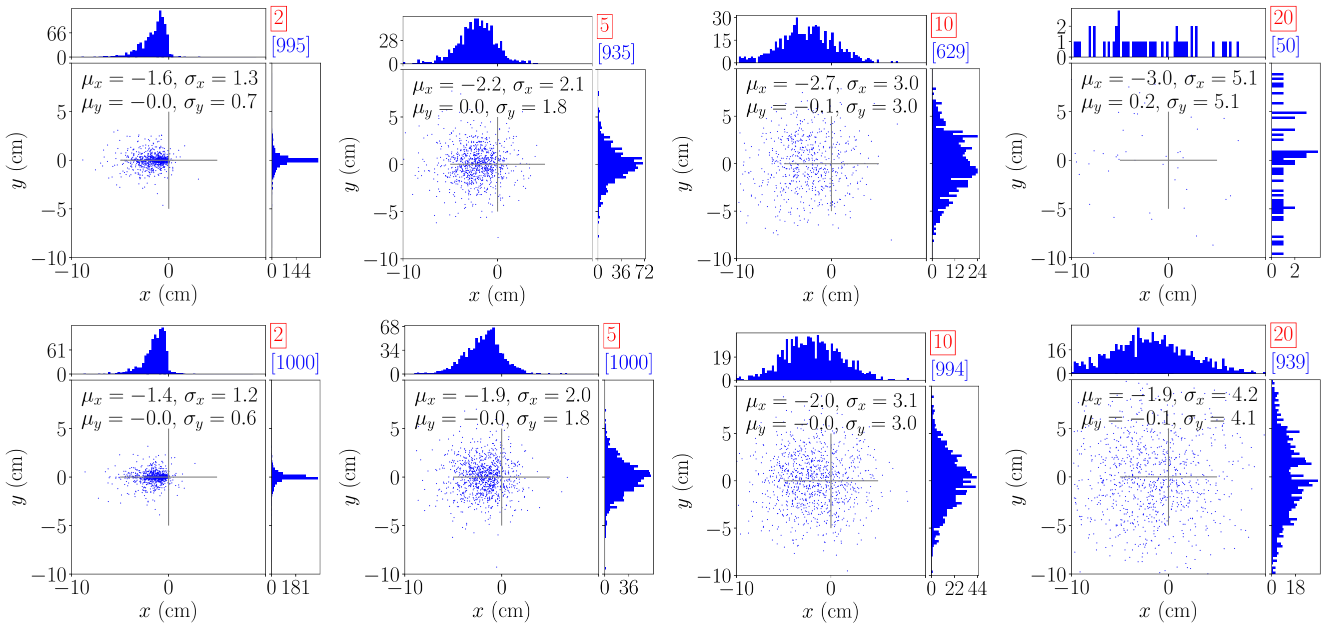

FIG. 8. Set of 4-keV neutrons directed along $\{-1, 0, 0\}$ were generated consecutively inside a large volume of plastic scintillator, doped at 1.5 wt % ^{6}Li (top row of plots) and undoped (bottom row of plots); the directional effect of the scattering they undergo prior to capture is shown after 2, 5, 10 and 20 scatters (a typical total for this material). Displacements in the *xy* plane; the gray cross (10 cm across) indicates the origin and the scale to make the displacement in the distributions more visible. For the undoped scintillator (bottom row), the neutrons undergo a higher number of scatters on average, making the displacement more obvious.

plans as *hybrid* designs. All of them seek to improve directional performance by incorporating space for the neutron to exit the target medium almost immediately after production and then undergo thermalization and capture in a different target segment, which is the driving behavior behind the directional capabilities of SANTA.

2. "Checkerboarding"

One of our primary approaches was to provide this free-flight space by simply removing alternating detector segments from the SANDD and NuLat 15^3 configurations in a "checkerboard" pattern. This pattern is determined by the row, column, and (in three dimensions) layer numbers for any given cell in the lattice. There are two types of cells in this arrangement.

(1) *Active* cells, which are occupied by a scintillator segment as usual.

(2) *Inert* cells, which are either left empty (air, vacuum, etc.) or, if necessary, are filled with some material which is effectively transparent to neutrons and (for some geometries) optical photons.

A lattice cell is made active if and only if its row, column, and (in three dimensions) layer numbers are all either simultaneously even or simultaneously odd: for 2D detectors, $ROW\% \ 2 = COL\% \ 2$; for 3D detectors, $ROW\% \ 2 = COL\% \ 2 = LYR\% \ 2$, where "%" is the modulus operator.

Renderings of our simulated versions of these arrangements are shown in Figs. 9 and 10. Note that the 3D version does not identically reproduce the traditional 2D checkerboard pattern in any single plane. Instead, it produces a pattern in which each active cube only has active neighbors at its vertices, rather than against its faces. This is the 3D analog to the traditional 2D checkerboard, wherein black squares only have black neighbors at their corners rather than along their sides. It is this "neighbors on vertices only" property that provides flight space for IBD neutrons within an otherwise bulk-volume detector.

For this study's simulations, all inert cells were simply left empty (i.e., they contained only air). We leave

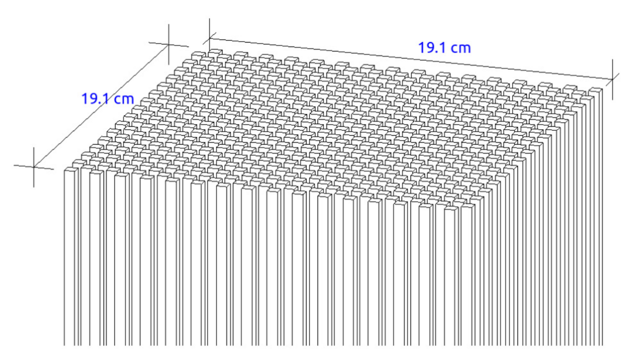

FIG. 9. Closeup showing 2D "checkerboard" lattice arrangement.

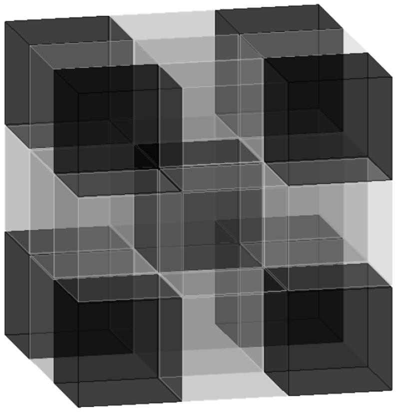

FIG. 10. Closeup showing 3D "checkerboard" lattice arrangement (inert cells ghosted).

the investigation of candidate inert materials to future work, other than to note the following. To qualify, a material's interaction lengths for both neutron elastic scattering and neutron capture should be at least comparable to (and ideally much larger than) the cell size: $\{\lambda_{es}, \lambda_{\text{cap}}\} \gtrsim \{l, w, h\}_{\text{cell}}$. If the inert cells also need to serve as light guides, such as in the NuLat/ROL arrangement, then the material must be sufficiently transparent to optical photons as well. We have run preliminary simulations indicating that glass/quartz (SiO_2) may be one such material.

D. Detector selection

Now that we have described each of the experiments we chose to simulate, we would like to briefly discuss why we selected this particular collection.

There are a number of experiments we could have chosen to represent each fundamental detector type. The field in general is well-represented in the 2015 survey of planned short-baseline reactor-antineutrino experiments listed in Table 1 of the NuLat whitepaper [26]. Most of the detectors in the table were designed for a simple measurement of the antineutrino flux and not for antineutrino directionality. As a result, our examination of one or two designs from each type, monolithic/minimally segmented (Double Chooz), 2D segmented (PROSPECT, SANDD), and 3D segmented (NuLat), covers the field of short-baseline reactor experiments as far as antineutrino directionality is concerned.

Because members of our group personally worked on the miniTimeCube (mTC), NuLat, and SANDD experiments, and our faculty includes members of the Double Chooz and PROSPECT collaborations, these detectors were naturally optimal choices for use in this study. The SANTA design is the only one of its type, so its inclusion was essentially predetermined. Finally, the hybrid designs appear here because they were developed by our group as part of this work.

E. Accuracy and angular resolution

We give the angular resolutions of these experiments in terms of $[\Delta\varphi]_{1\sigma}$, the 1σ uncertainty on the reconstructed source direction. It is the half-aperture of a cone in the 3D experiments and the half-angle of an arc in the 2D experiments. Following the formulation used by Double Chooz [44,45,54], we have calculated $[\Delta\varphi]_{1\sigma}$ as follows:

$$[\Delta\varphi]_{1\sigma} = \arctan\left(\frac{P/d_n}{\sqrt{N}}\right), \tag{3}$$

where $[\Delta\varphi]_{1\sigma}$ is the 1σ angular uncertainty on the reconstructed direction to the $\overline{\nu_e}$ source, P is the mean position resolution, d_n is the mean distance between the prompt and delayed events, and N is the number of IBD events used for direction reconstruction. (Recall from Sec. II A that

TABLE I. Summary. The total number of IBDs simulated in each detector is 10 000. Target material is PVT for all detectors except for Double Chooz. We use N_{trg} to represent the total number of IBD-candidate events registered by the antineutrino trigger. We use N_{1V} to denote the number of IBD-candidate events for which the prompt and delayed events occurred within a single volume/segment; these events were not used for directional reconstruction except in the monolithic (Chooz-type) detector. The resulting number of IBD-candidate events used for directional reconstruction is $N = N_{\text{trg}} - N_{1V}$. Here $\langle\cos\psi\rangle$ is somewhat a measure of angular accuracy, and $\Delta\varphi$ is the analytically-calculated 1σ angular uncertainty on the reconstructed direction to the antineutrino source: see Sec. III E; it is the half-aperture of a cone in the 3D experiments and the half-angle of an arc in the 2D experiments. Note that the 2D experiments are reconstructing the *azimuthal angle only*.

Recon. Type	Experiment	Dopant	wt %	Vol. (l)	P (mm)	d (mm)	N_{trg}	N_{1V}	N	$\langle\cos\psi\rangle$	φ (°)	$\Delta\varphi$ (°)
	DC (data)	Gd	0.1	10 000	156.7	16.7	8249	...	8249	0.059	7.4	5.90
	Monolithic	Gd	0.1	785 000	125.27	13.9	9198	...	9198	0.052	−2.55	5.37
3D	NuLat 5^3	^{6}Li	1.5	15.6	43.4	20.0	4592	661	3931	0.256	0.82	1.98
	3D Chkbd.	^{6}Li	1.5	107	105.7	32.7	4384	178	4206	0.194	6.03	2.85
	SANTA	B	0/5	24.0	218.28	1000	2275	0	2275	0.876	−0.56	0.26
	SANDD-CM	^{6}Li	1.5	0.64	16.8	10.0	250	3	247	0.360	12.08	6.10
2D	2D Chkbd.	^{6}Li	1.5	5.12	55.6	24.8	1864	4	1860	0.297	4.02	2.98
	PROSPECT	^{6}Li	0.08	3465	225.7	99.0	9489	5763	3726	0.335	3.03	3.82

$d_n \equiv \|\vec{S}_R\|$.) Here P is itself calculated via $P = (\sigma_x + \sigma_y + \sigma_z)/3$, where σ_x, σ_y, and σ_z are standard deviations for the displacement vector; in the monolithic case, it is the sigma of the Gaussian fit. For the 2D detectors, the calculation is as follows: $P = (\sigma_x + \sigma_y)/2$.

To specifically focus on the inherent potential directionality of each approach, we determined to *not* include backgrounds at this stage. The idea here, particularly for the SANTA design, was to investigate whether the (expected) improvement in directional capability offered sufficient reason to proceed to addressing the (expected) difficulties with backgrounds. Further details on each set are discussed in the following.

F. Shared parameters

We used RAT-PAC [55,56] (an implementation of GEANT4) and ROOT [57,58] for simulation and analysis; it was adapted by various collaborations including SNO+ [21] and AIT [59–61]. We simulated 10 000 IBD events in each detector. We took the $\overline{\nu_e}$ source to be distant enough that the incoming antineutrino flux could be well-represented by a plane wave; that is, we took the incoming antineutrinos to be uniform in direction. Furthermore, we took the $\overline{\nu_e}$ source to be located "at the horizon" relative to the detectors. For convenience, we placed our origins at the center of each detector with the x-axis pointing toward the $\overline{\nu_e}$ source, so that the incoming antineutrinos were traveling along $\{x, y, z\} = \{-1, 0, 0\}$. We then oriented each detector to be "facing" the $\overline{\nu_e}$ source; that is, we aligned each detector for its optimal directional sensitivity for the chosen antineutrino direction. The energy distribution for the IBD events was taken from the reactor spectrum built into RAT-PAC [55]. The IBD vertices were generated in a uniform (flat) random distribution throughout a volume or set of volumes chosen specifically for each detector. IBD events were separated in time by a Poisson distribution of mean 1 s. In all cases but NuLat 3^3, IBD vertices were distributed uniformly throughout the scintillator volume(s). In NuLat 3^3, IBD vertices were constrained to the central cube.

Backgrounds were expressly excluded from this study and will be addressed in subsequent work. This allows us a clear examination of the potential directional capability inherent to each geometry, with the goal of assessing which designs we wish to investigate further (including studies of performance in the presence of backgrounds). It also prevents our discussion from becoming needlessly restricted to a particular deployment setting, as background profiles are strongly site-dependent.

G. Reconstruction and event selection

For vertex reconstruction, we start with the raw Monte Carlo position. Then, for each $x_i \equiv \{x, y, z\}$:

(a) if the detector is segmented along x_i, we use x_i at the center of the segment; or
(b) if the detector is not segmented along x_i, we apply Gaussian noise to the raw Monte Carlo value according to the detector's estimated position resolution.

(For details on direction reconstruction, see Sec. II.)

Very little event selection was required for this study due to the configuration of our simulations. Because we generated only IBD events, there were no backgrounds to filter out. The IBDs were separated by a uniform 1-s interval, so they did not overlap in time. As a result, we needed only to consider the location of neutron capture.

(a) IBDs whose neutron was not captured in a detector target segment were discarded.
(b) All other IBDs were included in the total IBD count.

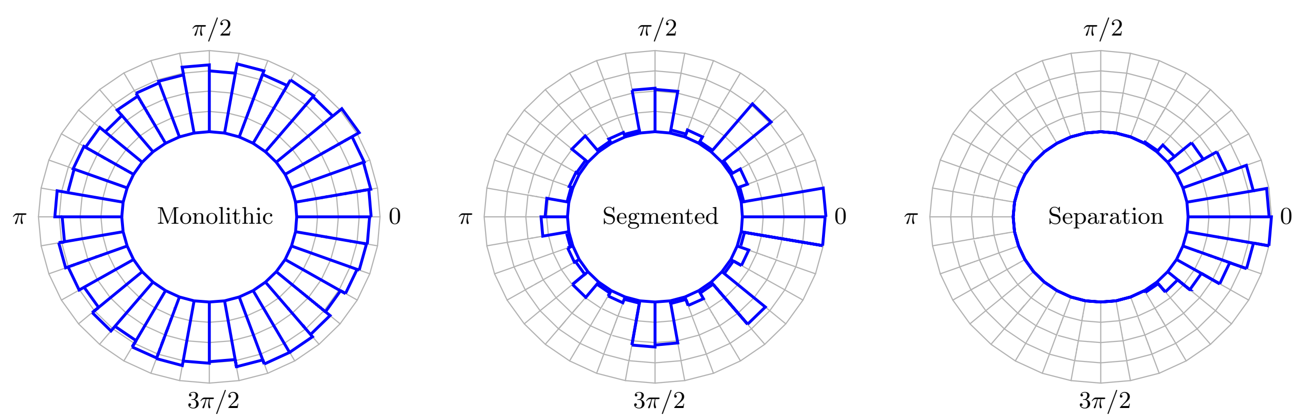

FIG. 11. Distributions of the azimuthal angle φ for three selected geometries: monolithic (Chooz), segmented (NuLat 5^3), and separation (Santa). The bin width is 10°; the inner circle on each histogram corresponds to 0 events and the outer circle is normalized to the max number of events per bin.

(c) Remaining IBDs that passed the single-volume cut were then used for direction reconstruction, as detailed in the caption of Table I.

During this process, we developed software tools for analysis and visualization that we hope will be useful to the community in general and to ROOT/RAT-PAC users in particular (see [56]). The results of these simulations are presented in Sec. IV.

IV. RESULTS

A summary of the main results from our primary simulation set is given in Table I.

A. Selected examples

We have chosen a trio of examples which highlight the behaviors of the three basic detector categories, shown in Fig. 11. The *monolithic*, *segmented*, and *separation* design types are represented by Double Chooz, NuLat5^3, and SANTA, respectively. It is worth noting that, although SANTA appears to have superior angular reconstruction, the separation concept in itself is rather a nonrealistic approach as it faces major background issues and the packing factor is rather small compared with all other designs: the target layer is subpercent of the total volume needed for this concept to work. This study was posited that the incoming antineutrino direction was perpendicular to the detector plane; thus, creating a bias in reconstructing the direction. We studied other orientations of the detector plane (which showed a degraded performance). We decided not to include them here as that would divert the reader's attention toward a rather unrealistic detector concept at the expense of giving other detector designs a similar amount of detail.

The scalability of designs incorporating this effect is limited by two closely related constraints.

(1) Along the direction of antineutrino travel, the thickness d_{active} of the detector's target segments should not significantly exceed the neutron-capture distance.

(2) Along this direction, some or all of these active segments should be followed by a sufficiently neutron-transparent region with a thickness d_{inert} that is at least comparable to the neutron-capture distance:

$$d_{\text{active}} \lesssim d_n \lesssim d_{\text{inert}} \tag{4}$$

B. Cosine results

The quantity $\cos\psi$ for a given event gives a value on the interval $[-1, +1]$ that reflects the degree of agreement between $\hat{S}_R$ and $\hat{S}_T$, as illustrated in Figs. 12 and 13. Values near -1 indicate a reconstructed direction pointing away from the true source direction; values near 0, perpendicular to the true source direction; and values near $+1$, toward the true source direction. Stated simply, distributions that are skewed more heavily to the right of these plots generally indicate better directional performance.

The $\cos\psi$ distributions for the 2D and 3D experiments are shown in Fig. 14. The base material (prior to doping) for all, but the monolithic (Chooz-type), detectors is our simulated version of PVT, which is the base polymer for EJ-254 scintillator [62,63]. The base material for the monolithic detector is our simulated version of the organic liquid scintillator of Double Chooz. The column "Vol." in the table is the detector's active target volume in liters. Recall that our Chooz-type tank is substantially larger than those used in the actual Double Chooz experiment. The capture plane and the inert checkerboard cells of SANTA are, by definition, not included. The 1σ angular uncertainty $[\Delta\varphi]_{1\sigma}$ on the reconstructed direction to the antineutrino source: see Sec. III E; it is the half-aperture of a cone in

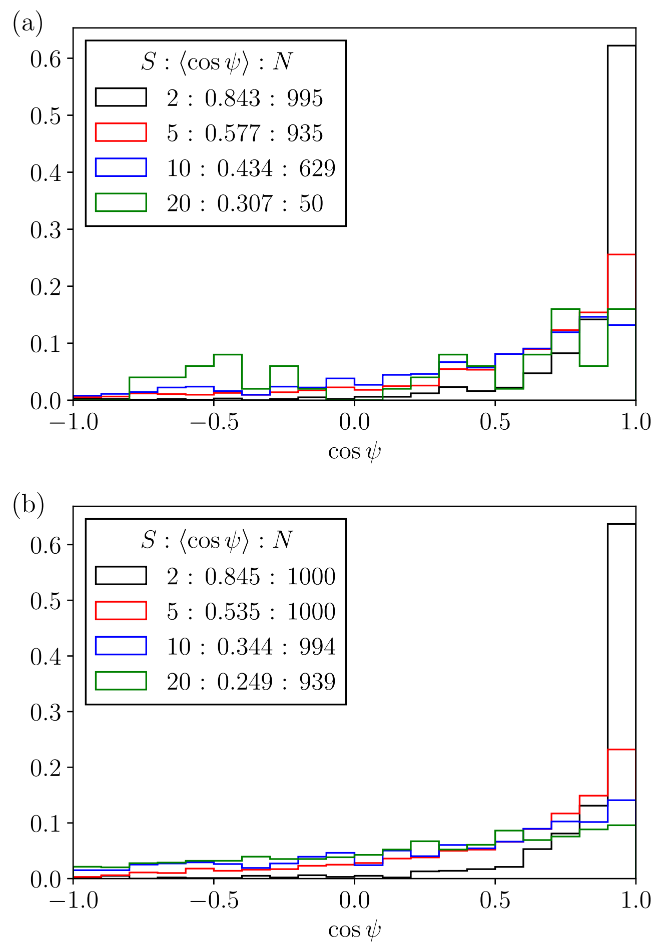

FIG. 12. Distribution of the $\cos\psi$ for various number of scatters (indicated in the legend along the mean values): (a) doped; (b) undoped. The mean values indicate the strength of the directional trend. Number of neutrons left after S number of scatters is indicated in the legend, i.e., the number of entries in the corresponding histogram.

the 3D experiments and the half-angle of an arc in the 2D experiments.

In order to show *only* the directional effects due to neutron scattering, we simulated a uniform set of 1000 neutrons with kinetic energy of 4 keV in a piece of plastic scintillator doped at 1.5 wt % ^{6}Li.

Figure 8 shows relevant parameters for these neutrons after 2, 5, 10 and 20 scatters. It is worth noting that all of these parameters, most notably the width of the spread and the total number of scatters, can vary substantially depending on the scintillator material, choice of dopant, and doping concentration. The raw Monte Carlo positions are shown in Fig. 8(a). After the first scatter, the distribution is quite clearly forward-biased, but it spreads out considerably in just a few more scatters. After 20 scatters, a typical total in this material, the distribution is only slightly heavier in the forward direction than in the backward direction, and the transverse spread is comparable to the forward-backward spread. Figure 8(b) shows a quantitative view of this process, representing the overall directional information via the distribution of $\cos\psi$ at each step. In $N = 2$, the momenta are strongly concentrated in a narrow cone about the initial momentum, but in $N = 5$, the cone is considerably broader and much less sharply defined. The stark contrast between $N = 2$ and $N = 5$ indicates how detrimental even a few scatters are to the directional information carried by the neutron. By the time the neutron captures at around $N = 20$, the trend in $\cos\psi$ is relatively weak. In a real detector with finite position resolution, as opposed to the MC-truth positions shown here, the reconstructed trend is weaker still.

The problem this causes in reconstructing the direction of the original incident $\overline{\nu_e}$ is that the position distributions in $\{x, y, z\}$ of the prompt and delayed events become a pair of closely overlapping Gaussians, both having standard deviations that are considerably larger than the separation between their means. This is another reason (in addition to the stochasticity discussed in Sec. II B) that many events are needed to resolve the source direction. This also indicates that improving the position resolution P of a traditional IBD detector can only increase its directional capability up to the point at which $P \sim d_n$, which is $\mathcal{O}(1\text{ cm})$ in the relevant materials.

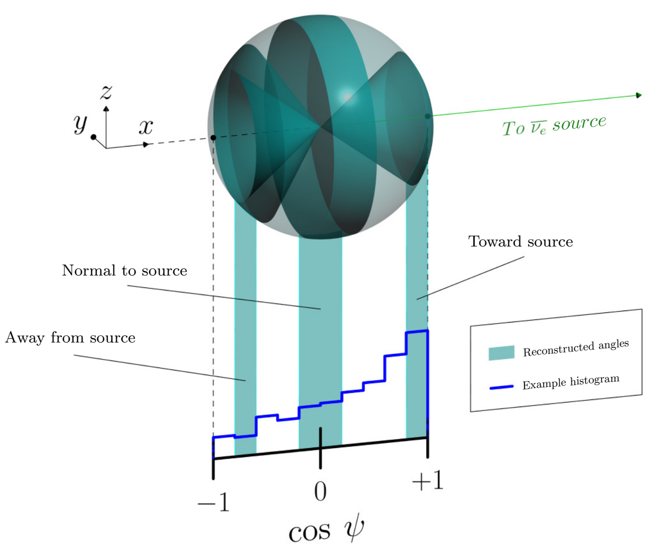

FIG. 13. Physical meaning of $\cos\psi$ distributions, illustrated here as it applies to the 3D experiments. The 2D analog is the projection of this diagram onto the *xy* plane. Events in the leftmost shaded region (i.e., the second bin from the left in the example histogram) correspond to reconstructed angles falling within the solid angle between the two cones defined by $\cos\psi = -0.8$ and $\cos\psi = -0.6$, or $\psi \approx 143^\circ$ and $\psi \approx 127^\circ$.

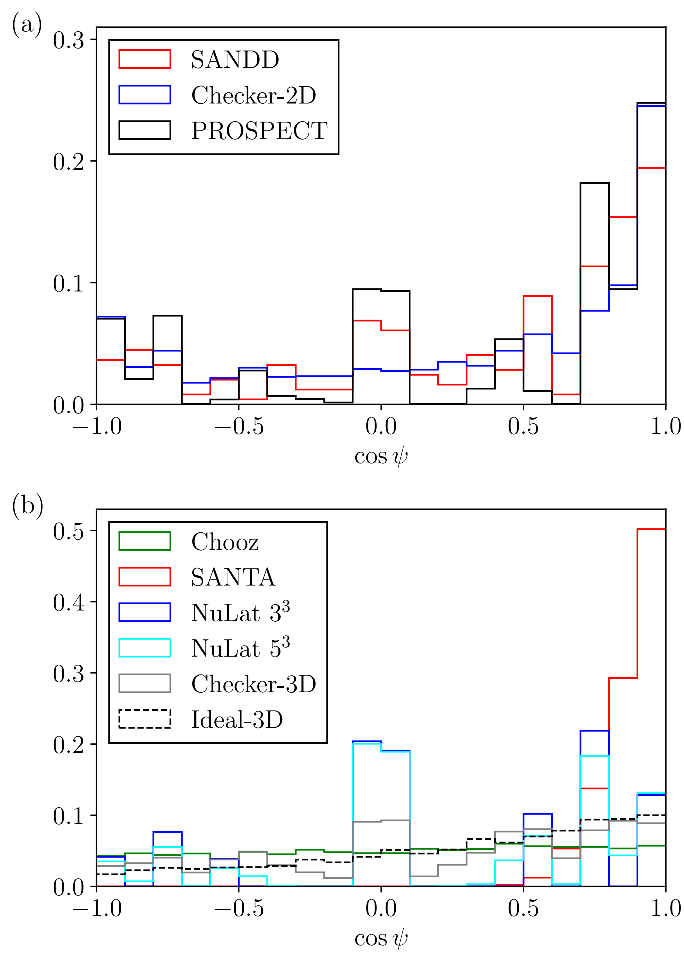

FIG. 14. Normalized distribution of $\cos\psi$ for (a) 2D and (b) 3D experiments. The Chooz-like monolithic detector is listed among the 3D detectors. The "Ideal-3D" distribution indicates the simulated directional performance of a 1.5-wt % ^{6}Li-loaded, monolithic detector with a hypothetical *perfect* position resolution (i.e., $\delta\{x, y, z\} \equiv 0$). It effectively represents the theoretical maximum directional performance of a nonsegmented detector (with this particular target material), due to the neutron-scattering problem discussed in Sec. III B.

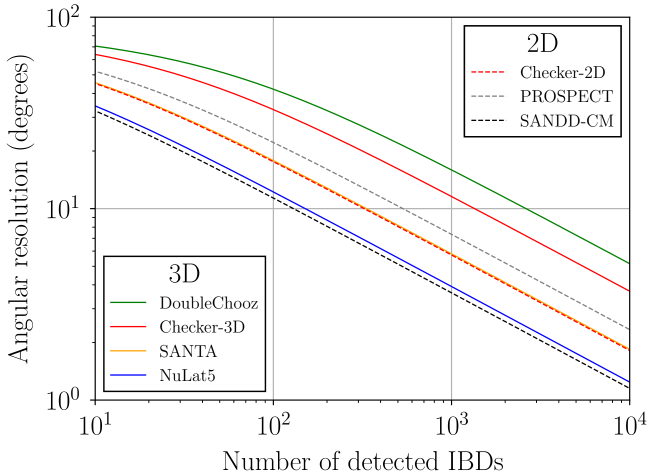

FIG. 15. Angular uncertainty $\Delta\varphi$ as a function of detected IBD events for various detector designs (2D detectors indicated by a dashed line; 3D detectors indicated by a solid line). The calculation is based on Eq. (5) using the values for the mean position resolution P and the mean distance d_n (between the prompt and delayed events) presented in Table I for the simulated detector geometries, as well as taking into account the packing factor Π.

C. Accounting for nonsensitive detector volume

To better understand various detector performance and not to give a reader misleading conclusion that SANTA is the best performing detector, we introduce a packing factor to roughly account for the void/insensitive volume in the detectors. For SANTA, it is only 0.46%, for Checkerboard-3D and -2D, 25% and 50%, respectively; for SANDD-CM, 70%; whereas other geometries are assumed to have a packing factor of 100%. We therefore modify Eq. (3) as follows:

$$[\Delta\varphi]_{1\sigma} = \arctan\left(\frac{P/d_n}{\sqrt{N\Pi}}\right), \tag{5}$$

where Π is the packing factor, and all other definitions remain unchanged. The resulting angular resolution is represented in Fig. 15.

V. CONCLUSION

We have shown how a variety of small existing and hypothetical IBD detectors can determine the incoming direction of electron-antineutrinos given a sufficient number of events. Our principal conclusions are as follows.

A. Solving neutron scattering

Directionality from near-surface reactor-IBD detectors can be improved substantially with currently existing technology. This requires designing the detector geometry to prioritize directional performance. The same is likely true for IBD detectors in other deployment scenarios as well. In addition, bulk-volume IBD detectors, regardless of segmentation or scale, are restricted substantially in their potential directional performance, even with continued improvements in vertex resolution. We have shown that is because they are inherently limited by the neutron-scattering problem as detailed in Sec. III B. As a result, IBD detectors intended for directional measurements will likely require a geometry incorporating some amount of open (or otherwise neutron-transparent) space for minimally scattered neutrons to traverse before undergoing thermalization and capture. These constraints, summarized in Eq. (4), should make it possible for the detector to surpass the performance limits imposed by the aforementioned neutron-scattering problem, with a performance improvement commensurate with the degree to which the constraints are satisfied or exceeded.

B. Future designs

As emphasized in our results presented in Fig. 15, this study strongly suggests that the field of antineutrino source-finding via IBD detection can make substantial improvements by employing novel geometries that are crafted to maximize directional performance, and we look for the next generation of detectors to expand what we can learn from the only class of elementary particle which preserves information about its point of origin. For example, in Fig. 15, the angular uncertainty $\Delta\varphi$ as a function of IBD events, by itself, clearly favors designs such as SANDD-CM and NuLat5. However, as discussed in Sec. III B, 3D directional reconstruction using physically realizable geometries are very likely still not worth the added cost and complexity. Two-dimensional reconstruction is much easier to attain and is sufficient for all likely nonproliferation applications of which we are currently aware. For example, the number of channels needed by SANDD-CM and NuLat5 are $\mathcal{O}(10^3, 10^2)$, respectively. Therefore, our current conclusion is that a PROSPECT-like design, with fewer channels and larger segments, is likely the most economical way to achieve angular resolutions on the order of a few degrees.

Nonproliferation scenarios further than $\mathcal{O}(10^2$ m) from a reactor, which are expected to require a fiducial mass $\gg 1$ ton, will likely be restricted to only 2D reconstruction, largely because of the scalability constraints discussed previously. We note that while the SANTA concept had better angular resolution *per event*, its relatively poor packing factor, and consequent small number of detected events per unit volume, means that its overall performance does not compare well with PROSPECT, SAND-CM, and NuLat-5. Checkerboarding is one possible method for hybridizing SANTA with more robust detectors, but other methods may provide equal or better directional benefit without the added complexity caused by the anisotropy inherent to the checkerboard lattice. On the technology side, although considered challenging in the past, new techniques have become available to support constructing finely segmented detectors, or detectors of mixed materials, such as 3D printing of ^{6}Li or ^{10}B PSD scintillators [64]. This is actively being pursued by the authors, with engineering of a detector at UH underway, and follow-on studies to be published soon.

ACKNOWLEDGMENTS

This work is supported by the US Department of Energy National Nuclear Security Administration and Lawrence Livermore National Laboratory [Contract No. DE-AC52-07NA27344, release number LLNL-JRNL-859999]. We wish to acknowledge the University of Hawai'i at Mānoa, the Department of Physics and Astronomy, and the HEP group in particular. We also thank engineering consultants Angela Mareschal and Ed Reedy. We thank Gabrielle Zacek and Viktor Zacek, the pioneers of the IBD directionality, for sharing the story of how the forward/backward asymmetry in IBD neutrons was first discovered in the Gösgen experiment. Last but not least, we acknowledge guidance provided by Adam Bernstein during the initial stages of this project.

[1] C. Cowan, F. Reines, F. Harrison, H. Kruse, and A. McGuire, Detection of the free neutrino: a confirmation, Science **124**, 103 (1956).

[2] F. Reines, M. F. Crouch, T. L. Jenkins, W. R. Kropp, H. S. Gurr, G. R. Smith, J. P. F. Sellschop, and B. Meyer, Evidence for high-energy cosmic ray neutrino interactions, Phys. Rev. Lett. **15**, 429 (1965).

[3] C. Achar, M. Menon, V. Narasimham, P. Murthy, B. Sreekantan, K. Hinotani, S. Miyake, D. Creed, J. Osborne, J. Pattison, and A. Wolfendale, Detection of muons produced by cosmic ray neutrinos deep underground, Phys. Lett. **18**, 196 (1965).

[4] R. Burns, K. Goulianos, E. Hyman, L. Lederman, W. Lee, N. Mistry, J. Rettberg, M. Schwartz, J. Sunderland, and G. Danby, Search for intermediate bosons in high-energy neutrino interactions, Phys. Rev. Lett. **15**, 42 (1965).

[5] R. Davis, D. S. Harmer, and K. C. Hoffman, Search for neutrinos from the Sun, Phys. Rev. Lett. **20**, 1205 (1968).

[6] A. A. Borovoi and L. A. Mikaelyan, Possibilities of the practical use of neutrinos, At. Energy **44**, 589 (1978).

[7] A. I. Afonin, S. A. Bogatov, A. G. Vershinskii, S. N. Ketov, Y. V. Klimov, B. I. Kopeikin, A. A. Kubshinnikov, A. A. Labzov, I. N. Machulin, L. A. Mikaelyan, K. V. Ozerov, V. V. Sinev, and S. V. Tolokonnikov, Electron antineutrino spectra at two distances from the reactor of the Rovno nuclear power plant: search for oscillations, JETP Lett. **45**, 247 (1987).

[8] K. Gabathuler, F. Boehm, F. von Feilitzsch, J. L. Gimlett, H. Kwon, R. L. Mossbauer, J. L. Vuilleumier, G. Zacek, and V. Zacek, A search for neutrino oscillations by measurement of the $\bar{\nu}_e$ spectra at two distances from a nuclear reactor, Phys. Lett. B **138**, 449 (1984).

[9] J. F. Cavaignac, A. Hoummada, D. H. Koang, B. Vignon, Y. Declais, H. de Kerret, H. Pessard, and J. M. Thenard, Indication for neutrino oscillation from a high statistics experiment at the Bugey reactor, Phys. Lett. B **148**, 387 (1984).

[10] G. S. Vidyakin, V. N. Vyrodov, Y. V. Kozlov, A. V. Martem'yanov, V. P. Martem'yanov, A. N. Odinokov, S. V. Sukhotin, V. G. Tarasenkov, E. V. Turbin, *et al.*, Limitations on the characteristics of neutrino oscillations, JETP Lett. **59**, 390 (1994).

[11] Z. D. Greenwood, W. R. Kropp, M. A. Mandelkern, S. Nakamura, E. L. Pasierb-Love, L. R. Price, F. Reines, S. P. Riley, H. W. Sobel, N. Baumann, and H. S. Gurr, Results of a two position reactor neutrino oscillation experiment, Phys. Rev. D **53**, 6054 (1996).

[12] Y. Fukuda, T. Hayakawa, E. Ichihara, K. Inoue, K. Ishihara, H. Ishino, Y. Itow, T. Kajita, J. Kameda, S. Kasuga, *et al.*, (Super-Kamiokande Collaboration), Evidence for oscillation of atmospheric neutrinos, Phys. Rev. Lett. **81**, 1562 (1998).

[13] Q. R. Ahmad, R. C. Allen, T. C. Andersen, J. D. Anglin, G. Bühler, J. C. Barton, E. W. Beier, M. Bercovitch, J. Bigu, S. Biller, *et al.*, (SNO Collaboration), Measurement of the rate of $\nu_e + d \rightarrow p + p + e^-$ interactions produced by ^{8}B solar neutrinos at the Sudbury Neutrino Observatory, Phys. Rev. Lett. **87**, 071301 (2001).

[14] B. Aharmim, S. N. Ahmed, A. E. Anthony, N. Barros, E. W. Beier, A. Bellerive, B. Beltran, M. Bergevin, S. D. Biller, K. Boudjemline, *et al.*, Combined analysis of all three phases of solar neutrino data from the Sudbury Neutrino Observatory, Phys. Rev. C **88**, 025501 (2013).

[15] K. Eguchi, S. Enomoto, K. Furuno, J. Goldman, H. Hanada, H. Ikeda, K. Ikeda, K. Inoue, K. Ishihara, W. Itoh, *et al.*, (KamLAND Collaboration), First results from KamLAND: evidence for reactor antineutrino disappearance, Phys. Rev. Lett. **90**, 021802 (2003).

[16] E. Christensen, P. Huber, P. Jaffke, and T. E. Shea, Antineutrino monitoring for heavy water reactors, Phys. Rev. Lett. **113**, 042503 (2014).

[17] A. Bernstein, N. Bowden, B. L. Goldblum, P. Huber, I. Jovanovic, and J. Mattingly, Colloquium: Neutrino detectors as tools for nuclear security, Rev. Mod. Phys. **92**, 011003 (2020).

[18] M. Andriamirado, B. Balantekin, C. D. Bass, O. B. Rodrigues, E. P. Bernard, N. S. Bowden, C. D. Bryan, R. Carr, T. Classen, A. J. Conant, *et al.*, (PROSPECT Collaboration), Reactor antineutrino directionality measurement with the PROSPECT-I detector, ArXiv:2406.08359.

[19] M. Andriamirado, A. B. Balantekin, C. D. Bass, D. E. Bergeron, E. P. Bernard, N. S. Bowden, C. D. Bryan, R. Carr, T. Classen, *et al.*, (PROSPECT Collaboration), Final measurement of the ^{235}U antineutrino energy spectrum with the PROSPECT-I detector at HFIR, Phys. Rev. Lett. **131**, 021802 (2023).

[20] F. P. An, W. D. Bai, A. B. Balantekin, M. Bishai, S. Blyth, G. F. Cao, J. Cao, J. F. Chang, Y. Chang, H. S. Chen, *et al.*, ((Daya Bay Collaboration), Precision measurement of reactor antineutrino oscillation at kilometer-scale baselines by Daya Bay, Phys. Rev. Lett. **130**, 161802 (2023).

[21] A. Allega, M. R. Anderson, S. Andringa, J. Antunes, M. Askins, D. J. Auty, A. Bacon, N. Barros, F. Barão, R. Bayes, *et al.*, (The SNO+ Collaboration), Evidence of antineutrinos from distant reactors using pure water at SNO+, Phys. Rev. Lett. **130**, 091801 (2023).
[22] G. Mention, M. Fechner, T. Lasserre, T. Mueller, D. Lhuillier, M. Cribier, and A. Letourneau, The reactor antineutrino anomaly, Phys. Rev. D **83**, 073006 (2011).
[23] J. Ashenfelter, A. B. Balantekin, H. R. Band, G. Barclay, C. Bass, N. S. Bowden, C. D. Bryan, J. J. Cherwinka, R. Chu, T. Classen, *et al.*, (PROSPECT Collaboration), PROSPECT—a precision reactor oscillation and spectrum experiment at short baselines, ArXiv:1309.7647.
[24] Y. Abreu, Y. Amhis, L. Arnold, G. Ban, W. Beaumont, M. Bongrand, D. Boursette, J. Buhour, B. Castle, K. Clark, *et al.*, (SoLid Collaboration), A novel segmented-scintillator antineutrino detector, JINST **12**, P04024 (2017).
[25] A. Haghighat, P. Huber, S. Li, J. M. Link, C. Mariani, J. Park, and T. Subedi, Observation of reactor antineutrinos with a rapidly-deployable surface-level detector, Phys. Rev. Appl. **13**, 034028 (2020).
[26] C. Lane, S. M. Usman, J. Blackmon, C. Rasco, H. P. Mumm, D. Markoff, G. R. Jocher, R. Dorrill, M. Duvall, J. G. Learned, *et al.*, A new type of neutrino detector for sterile neutrino search at nuclear reactors and nuclear nonproliferation applications, ArXiv:1501.06935.
[27] I. Alekseev, V. Belov, V. Brudanin, M. Danilov, V. Egorov, D. Filosofov, M. Fomina, Z. Hons, A. Kobyakin, D. Medvedev, *et al.*, DANSSino: a pilot version of the DANSS neutrino detector, Phys. Part. Nucl. Lett. **11**, 473 (2014).
[28] S. Oguri, Y. Kuroda, Y. Kato, R. Nakata, Y. Inoue, C. Ito, and M. Minowa, Reactor antineutrino monitoring with a plastic scintillator array as a new safeguards method, Nucl. Instrum. Meth. **A757**, 33 (2014).
[29] V. Kopeikin, M. Skorokhvatov, and O. Titov, Reevaluating reactor antineutrino spectra with new measurements of the ratio between ^{235}U and ^{239}Pu β spectra, Phys. Rev. D **104**, L071301 (2021).
[30] T. Akindele, N. Bowden, R. Carr, A. J. Conant, M. Diwan, A. Erickson, M. P. Foxe, B. L. Goldblum, P. Huber, I. Jovanovic, *et al.*, Nu tools: exploring practical roles for neutrinos in nuclear energy and security, ArXiv:2112.12593.
[31] T. Akindele, T. Anderson, E. Anderssen, M. Askins, M. Bohles, A. J. Bacon, Z. Bagdasarian, A. Baldoni, A. Barna, N. Barros, *et al.*, A call to arms control: synergies between nonproliferation applications of neutrino detectors and large-scale fundamental neutrino physics experiments, ArXiv:2203.00042.
[32] D. L. Danielson, O. A. Akindele, M. Askins, M. Bergevin, A. Bernstein, J. Burns, A. Carroll, J. Coleman, R. Collins, C. Connor, *et al.*, Directionally accelerated detection of an unknown second reactor with antineutrinos for mid-field nonproliferation monitoring, ArXiv:1909.05374.
[33] K. A. Hochmuth, M. Lindner, and G. G. Raffelt, Exploiting the directional sensitivity of the Double Chooz near detector, Phys. Rev. D **76**, 073001 (2007).
[34] E. Houston, O. Akindele, M. Bergevin, A. Bernstein, S. Dazley, and S. Bogetic, A neutrino detector design for safeguarding small modular reactors, ArXiv:2308.01306.
[35] D. Danielson, in *Applied Antineutrino Physics 2018 Proceedings*, ArXiv:1911.06834.
[36] P. Vogel and J. F. Beacom, Angular distribution of neutron inverse beta decay, $\vec{\nu}_e + p \to e^+ n$, Phys. Rev. D **60**, 053003 (1999).
[37] M. Zucker, R. Dragoset, and A. Kishore, Elemental data index (1999).
[38] G. Knoll, *Radiation Detection and Measurement* (Wiley, 2000).
[39] T. Tanaka, K. Hagiwara, E. Gazzola, T. Sudo, M. S. Reen, A. Ali, I. Ou, R. Dhir, P. K. Das, Y. Koshio, *et al.*, Gamma ray spectra from thermal neutron capture on gadolinium-155 and natural gadolinium, ArXiv:1907.00788.
[40] K. Hagiwara, T. Yano, T. Tanaka, M. S. Reen, P. K. Das, S. Lorenz, I. Ou, T. Sudo, Y. Yamada, T. Mori, T. Kayano, *et al.*, Gamma-ray spectrum from thermal neutron capture on gadolinium-157, Prog. Theor. Exp. Phys. **2019**, 023D01 (2019).
[41] G. Zacek, Search for neutrino oscillations at a fission reactor, Ph.D. thesis, Munich University of Technology, 1984, available online at https://inspirehep.net/literature/208723.
[42] F. Boehm, J. Busenitz, B. Cook, G. Gratta, H. Henrikson, J. Kornis, D. Lawrence, K. B. Lee, K. McKinny, L. Miller, *et al.*, Results from the Palo Verde neutrino oscillation experiment, Phys. Rev. D **62**, 072002 (2000).
[43] M. Apollonio, A. Baldini, C. Bemporad, E. Caffau, F. Cei, Y. Déclais, H. de Kerret, B. Dieterle, A. Etenko, L. Foresti, *et al.* ,(CHOOZ Collaboration), Determination of neutrino incoming direction in the CHOOZ experiment and supernova explosion location by scintillator detectors, Phys. Rev. D **61**, 012001 (2000).
[44] E. Caden, Studying neutrino directionality with the Double Chooz experiment, Ph.D. thesis, Drexel University, 2013, available online at https://doi.org/10.17918/etd-4167.
[45] E. Caden, (Double Chooz Collaboration), Studying neutrino directionality with Double Chooz, ArXiv:1208.3628.
[46] G. Bak, J. H. Choi, H. I. Jang, J. S. Jang, S. H. Jeon, K. K. Joo, K. Ju, D. E. Jung, J. G. Kim, J. H. Kim, *et al.*, (RENO Collaboration), Fuel-composition dependent reactor antineutrino yield at RENO, Phys. Rev. Lett. **122**, 232501 (2019).
[47] Y. Abe, J. C. dos Anjos, J. C. Barriere, E. Baussan, I. Bekman, M. Bergevin, T. J. C. Bezerra, L. Bezrukov, E. Blucher, C. Buck, *et al.*, (Double Chooz Collaboration), Improved measurements of the neutrino mixing angle θ_{13} with the Double Chooz detector, JHEP **1410**, 086 (2014).
[48] G. Bellini, J. Benziger, D. Bick, G. Bonfini, D. Bravo, M. B. Avanzini, B. Caccianiga, L. Cadonati, F. Calaprice, P. Cavalcante, *et al.*, (Borexino Collaboration), Cosmogenic backgrounds in Borexino at 3800 m water-equivalent depth, JCAP **1308**, 049 (2014).
[49] F. An, Q. An, J. Bai, A. Balantekin, H. Band, W. Beriguete, M. Bishai, S. Blyth, R. Brown, G. Cao, *et al.*, (Daya Bay Collaboration), A side-by-side comparison of Daya Bay antineutrino detectors, Nucl. Instrum. Meth. **A685**, 78 (2012).
[50] X. Ding, Development and calibration of NuLat, a new type of neutrino detector, Ph.D. thesis, Virginia Polytechnic Institute and State University, 2017, available online at https://vtechworks.lib.vt.edu/items/421dd278-6edf-4cf3-8305-69b3d75431ec.
[51] F. Sutanto, T. Classen, S. Dazeley, M. Duvall, I. Jovanovic, V. Li, A. Mabe, E. Reedy, and T. Wu, SANDD: a directional

antineutrino detector with segmented ^{6}Li-doped pulse-shape-sensitive plastic scintillator, Nucl. Instrum. Meth. **A1006**, 165409 (2021).

[52] K. Keefe, H. Alhajaji, E. Brubaker, A. Druetzler, A. Galindo-Tellez, J. Learned, P. Maggi, J. J. Manfredi, K. Nishimura, B. P. Souza, J. Steele, M. Sweany, and E. Takahashi, Design and characterization of an optically segmented single volume scatter camera module, IEEE Trans. Nucl. Sci. **69**, 1267 (2022).

[53] B. R. Safdi and B. Suerfu, Directional antineutrino detection, Phys. Rev. Lett. **114**, 071802 (2015).

[54] C. Langbrandtner, Background, sensitivity and directionality studies for the Double Chooz experiment, Ph.D. thesis, Heidelberg University, 2011, available online at http://hdl.handle.net/11858/00-001M-0000-0011-F08F-4.

[55] S. Seibert, C. Tunnell, J. Klein, M. Worcester, T. Bolton, W. Seligman, S. Sekula, and G. O. Gann, (Braidwood Collaboration), RAT–RAT is an analysis tool, https://github.com/rat-pac/rat-pac (2006), p. v8395950.

[56] M. Duvall, Tools for reactor-antineutrino studies in RAT-PAC, https://github.com/duvall3/rat-pac, 2022, v1.2.0/RAT v6c50cc3.

[57] R. Brun and F. Rademakers, in *Proceedings AIHENP'96 Workshop, Lausanne, September 1996* (1997), Vol. 389, p. 81.

[58] R. Brun and F. Rademakers, Root 5, https://root.cern/releases/release-53430, 2015, v5.34/30.

[59] V. A. Li, S. A. Dazeley, M. Bergevin, and A. Bernstein, Scalability of gadolinium-doped-water Cherenkov detectors for nuclear nonproliferation, Phys. Rev. Appl. **18**, 034059 (2022).

[60] L. Kneale, S. Wilson, T. Appleyard, J. Armitage, N. Holland, and M. Malek, Sensitivity of an antineutrino monitor for remote nuclear reactor discovery, Phys. Rev. Appl. **20**, 034073 (2023).

[61] O. Akindele, A. Bernstein, M. Bergevin, S. Dazeley, F. Sutanto, A. Mullen, and J. Hecla, Exclusion and verification of remote nuclear reactors with a 1-kiloton Gd-doped water detector, Phys. Rev. Appl. **19**, 034060 (2023).

[62] EJ-254, Scintillator EJ-254 data sheet, https://eljentechnology.com/products/plastic-scintillators/ej-254.

[63] D. Drake, W. Feldman, and C. Hurlbut, New electronically black neutron detectors, Nucl. Instrum. Meth. **A247**, 576 (1986).

[64] Y. Kim, N. Zaitseva, M. J. Ford, L. Carman, A. Glenn, M. Febbraro, and P. Hausladen, 3D printable polyvinyltoluene-based plastic scintillators with pulse shape discrimination, Nucl. Instr. Meth. **1055**, 168537 (2023).